# Chapter V
# Optical Properties of ZnS Nanoparticles and Effect of Doping with d Block Elements (Transition Elements)

Zinc sulphide (ZnS) is one of the first semiconductors discovered [1] and it has traditionally shown remarkable fundamental properties versatility and a promise for novel diverse applications, including light-emitting diodes (LEDs), electroluminescence, flat panel displays, infrared windows, sensors, lasers, and biodevices, etc.

This chapter focuses on the synthesis of Zinc sulphide nanoparticles in organic phase. XRD characterization and TEM measurements were done to study the structure of ZnS nanoparticles. The UV-Vis absorption spectrum, Photoluminescence measurements and FTIR measurements were done to study the optical properties. Malvern's Particle size distribution is studied to evaluate the size of the synthesized nanoparticles. Subsequently, phase transferred ZnS nanoparticles were doped with various levels of manganese and yttrium and effect of doping on the various characteristics were analyzed.

In this chapter, a very simple method of synthesizing ZnS, ZnMnS and ZnYS nanoparticles in organic phase at ambient room temperatures is discussed.

## 5.1 Introduction

ZnS has two commonly available allotropes - one with a Zinc Blende Structure (ZB) and another with a Wurtzite Structure (WZ). The figure shows the structure of Zinc blende and Wurtzite forms. Zinc blende form is the cubic form and the Wurtzite is hexagonal.

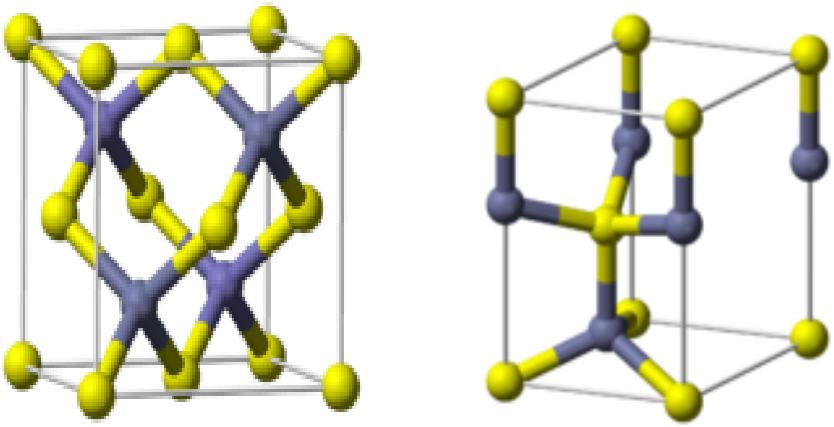

**A** **B**

**Fig 5.1** *Schematic showing Zincblende(A) and Wurtzite(B) crystal structure in ZnS*

ZnS has a large bandgap of approximately 3.72 eV and 3.77 eV (for cubic zinc blende (ZB) and hexagonal wurtzite (WZ) ZnS, respectively) and therefore it is more suitable for visible-blind ultraviolet (UV)-light based devices such as sensors/ photodetectors. The band structure of a solid describes ranges of energy levels that an electron is ‘‘forbidden’’ or ‘‘allowed’’ to have and it determines important electronic and optical properties of the material.

The optical properties of nanocrystalline semiconductor have been studied extensively in the past decades [2-5]. These materials behave differently from bulk semiconductors. With decrease in particle size, the band structure of the semiconductor changes, the band gap increases and the edges of band split into discrete energy levels called Quantum-confinement effects [7]. It is well-known that the optical and electronic properties change dramatically due to quantum confinement

of the charge carriers within the particle [8, 9]. ZnS, which is an important wide band gap semiconductor, has attracted attention owing to its wide application including UV light emitting diodes, organic LEDs, efficient phosphors in flat panel display, photovoltaic devices etc [10].

The photoluminescence mechanism of ZnS nanocrystals doped with other metal ions is very complex. Small particles have higher surface to volume ratio and hence have more accessible carriers for photoluminescence [11].

The surface states are very important for the physical properties and optical properties of nanoparticles. Usually, two emissions are observed from semiconductor nanoparticles – excitonic and trapped luminescence [12]. The excitonic emission is sharp and is located near the absorption edge of the particles, while the trapped emission is broad and is stokes shifted. Only the trapped luminescence arising from the surface states is observed in the ZnS nanoparticles [11].

To utilize semiconductor nanostructures as building blocks of functional nanodevices, it is important to synthesize the nanoparticles having diverse physical properties. This could be realized via appropriate doping.

Transition metal ions doped ZnS nanoparticles are the most popular materials for research in semiconductor nanocrystals. Doped nanocrystals of semiconductor can yield high luminescence [12]. These results suggested that doped semiconductor nanocrystals form a new class of luminescent materials, with a wide range of applications in e.g. displays, sensors and lasers [13]. To account for the new phenomena, Bhargava et al [12] suggested that with decreasing particle size a strong hybridization of the s-p states of the ZnS host and the d states of the $Mn^{2+}$ impurity must occur. This hybridization results in a faster energy transfer between the ZnS host and $Mn^{2+}$ impurity, yielding higher quantum efficiency.

The $Mn^{2+}$ ion, used as a dopant in many luminescent materials, has a $d^5$ configuration. The $Mn^{2+}$ ions exhibit a broad emission peak, whose position depends strongly on the host lattice due to the changes in the crystal field strength with host. The emission colour can vary from green to deep red corresponding to a $^4T_1$ -$^6A_1$ transition [14]. Bulk ZnS : Mn has been widely used as a phosphor, particularly in different electroluminescence devices. $Mn^{2+}$ d-electron states act as efficient luminescent centres while interacting strongly with s-p electronic states of the ZnS host into which external electronic excitation is normally directed. The subsequent transfer of electron and hole pairs into the electronic level of the $Mn^{2+}$ ion leads to the characteristic yellow-orange emission from the $Mn^{2+}$ $4_{T1}$-$^6A_1$ transition.

## 5.2 Experimental Details

**Chemicals:**

All the chemicals used were of analytical grade and were used as received without further purification.

$Zn(NO_3)_2$ - Zinc Nitrate

$C_{18}H_{36}O_2$ - Stearic Acid

$CHCl_3$ - Chloroform

$C_{18}H_{38}S$ - Octadecane Thiol

$MnCl_2$ - Manganese Chloride

$Y_2(CO_3)_3$ - Yttrium Carbonate

**Sample Preparation:**

For synthesis, 50 mL of $10^{-3}$M aqueous $Zn(NO_3)_2$ solution whose pH was adjusted to 8.5 was mixed with 50mL of $10^{-3}$M stearic acid dissolved in chloroform.

The mixture is stirred vigorously using a magnetic stirrer for 5 hours at room temperature.

This leads to the transfer of the Zinc ions from the aqueous phase to the organic phase. The phase transferred Zinc ions present in organic medium were separated from the stirred solution using a separating funnel.

Equal volumes of phase transferred zinc ions and 5 x $10^{-3}$ M ODT dissolved in chloroform were added. ODT behaves as a capping agent so that the cadmium ions do not agglomerate.

For standardizing the method of preparation various pH concentrations were experimented. However, for a pH concentration of 8.5, agglomeration was not observed. However, for any pH concentration between 8-9, it was observed that zinc ions were transferred to the organic phase. The stability of the CdS nanocrystals synthesized was very good for a pH concentration of 8.5. Similarly, the concentration of the capping agent (0.001 M -0.009M) was also varied to optimize the levels of the ODT used for stabilizing the nanocrystals.

The solutions were mixed well by shaking and the mixture was kept aside for 15 minutes. Then $H_2S$ gas was bubbled through the mixture for 15 minutes. As the reaction proceeds, a yellow coloration is observed in the solution, indicating the formation of ZnS nanoparticles in the organic phase.

For Manganese-doping, the corresponding aqueous salts of Mn and Zn were homogenously mixed in required weight proportions.$10^{-3}$M solution of $MnCl_2$ in proportions of 2%, 4%, 6%, 8%, and 10% in weight are prepared and added along with $Zn(NO_3)_2$ solutions.

Similarly, for doping with yttrium, $10^{-3}$M solution of yttrium carbonate dissolved in acidic distilled water and added in proportions of 2%, 4%, 6%, 8% &

10% in weight are prepared and added with $Zn(NO_3)_2$ solution and the same procedure is followed.

Very stable ZnS , $Zn_{1-x}Mn_xS$ and ZnYS nanocrystals in organic phase with ODT as the capping agents were obtained and the samples were characterized using different techniques.

## 5.3 UV-Visible Spectroscopy

The preparation produces ZnS quantum dots whose structures, composition and electronic structure are well characterized. The room temperature UV-Vis spectra of ZnS nanopartcles is shown in curve 1 of fig 5.2(B).

It can be seen that the strongest absorption peak of the as prepared sample appears at around 212 nm, and the absorption edge at 280 nm which is fairly blue shifted from the absorption edge of bulk ZnS (345 nm).

ZnS has good absorption for light in the wavelength of 220-350 nm [15] and this peak position reflects the bandgap of the particles. The fundamental absorption, which corresponds to electron excitation from the valence band to conduction band, can be used to determine the nature and value of the optical bandgap of the prepared ZnS nanoparticles. This blue shifted absorption edge is due to small size of the particles [7].

Semiconductor crystallites in the diameter range of a few nanometers show a three dimensional quantum size effect in their electronic structure. The quantum size effects on the band gap absorption energy can be measured by UV-Vis absorption spectroscopy.

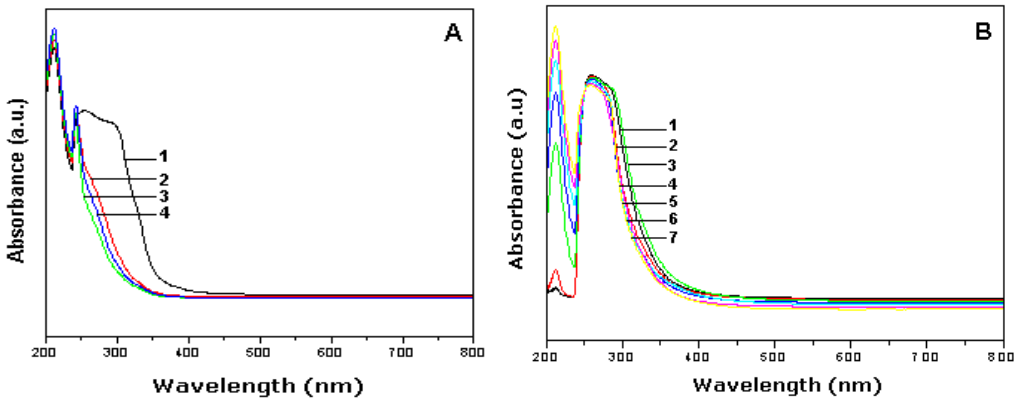


**Fig. 5.2(A)** *shows the UV-visible absorption spectrum of 2% by wt Mn doped ZnS nanoparticles(1), 5% by wt Mn doped ZnS nanoparticles (2), 8% by wt Mn doped ZnS nanoparticles (3), 10% by wt Mn doped ZnS nanoparticles (4).*

**Fig. 5.2(B)** *shows UV-visible absorption spectrum of undoped ZnS nanoparticles (1) and different levels of doping by wt with yttrium 2% (2), 4% (3),6% (4), 8% (5), 10% (6), 12% (7).*

Fig. 5.2(A) represents the absorption spectrum Zinc sulphide nanoparticles doped with different proportions by weight of manganese.

The absorption spectra are recorded in the range of 200-800 nm at room temperature. A strong absorption peak at 215 nm is assigned to the optical transition of the first excitonic state of the Mn doped ZnS nanoparticles and its narrow shape is an evidence of the very small size of the dispersed particles. The maximum absorption edge for the sample is observed at 320 nm which indicate a 25 nm blue shift from the bulk (345 nm). This blue shifted absorption edge is due to the small size of the particles. By Doping with manganese ions, the wavelength of absorption edge shift towards a higher wavelength compared to ZnS nanoparticles. This changes the band gap energy suggesting that there is direct energy transfer between semiconductor excited states and 3d levels of the $Mn^{2+}$ ions, that are coupled by energy transfer process [16].

Fig 5.2 (B) represents the absorption spectrum of yttrium doped nanoparticles with different concentrations of yttrium (curve 2-curve7).

The Yttrium doped ZnS absorption spectrum shows a strong absorption peak at 210 nm. This is attributed to the optical transition of the excitonic state and its narrow shape is an evidence of its small size of the dispersed particles. The maximum absorption edge for the sample is observed at 334 nm which indicates a 10-15 nm shift from the bulk. The absorption spectrum exhibits multiple peaks. There is no significant variation in the absorption levels when the doping levels are varied.

## 5.4 X-ray Diffraction (XRD)

XRD pattern of the phase transferred ZnS nanoparticles in organic phase, $Mn^{2+}$ doped ZnS (ZnS:Mn) and $Y^{3+}$ doped ZnS (ZnS:Y) were obtained and are shown in fig 5.3(A), 5.3(B) and 5.3(C) respectively. The diffraction analysis of the drop coated film on silicon substrates of the organic phase transferred Zinc sulphide nanocrystals, $Zn_{(1-x)}$ $Mn_xS$ nanoparticles and ZnYS nanoparticles was carried out on an Xpert PANalytical instrument operating at operating at 40 kV and a current of 30 mA with $CuK_\alpha$ radiation. These patterns have been recorded within the range of 30˚ - 70˚ with a scan rate of 2˚ / min.

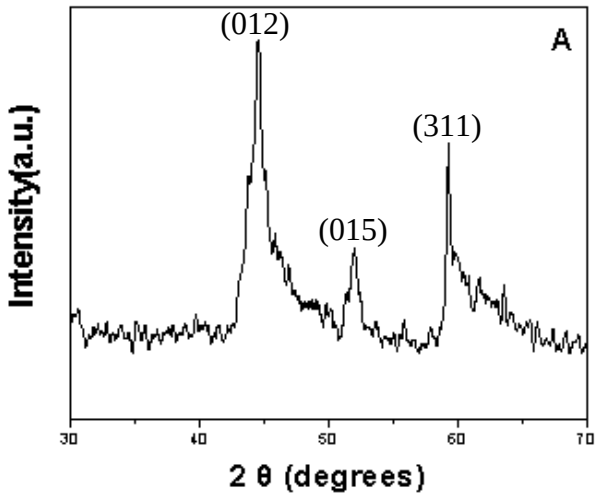


**Fig. 5.3(A)** *XRD pattern of drop coated film on Si substrate from synthesized ZnS nanoparticles. The Bragg reflections are indexed.*

It is seen that all the XRD peaks of the nanoparticles can be indexed as Zinc blende structure. It can be seen that the XRD patterns are broadened with two main peaks corresponding to (012) and (311) lattice planes. Fig. 5.3(B) shows the XRD pattern of $Zn_{0.95}$ $Mn_{0.05}$ S nanocrystals synthesized in organic phase. The zincblende phase persists up to 5%-Mn alloying with the ZnS nanocrystals. Thus, 5% Mn concentration seems to be perfect for the homogenous formation of alloyed $Zn_{1-x}$ $Mn_x$ S nanocrystals under ambient conditions.

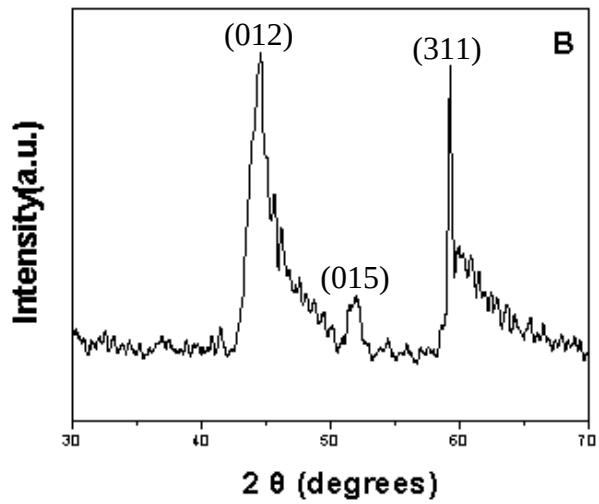


**Fig. 5.3(B)** *XRD pattern of drop coated film on Si substrate obtained from $Zn_{0.95}$ $Mn_{0.05}$S nanocrystals. The Bragg reflections are indexed.*

Fig. 5.3(C) shows the XRD pattern of ZnYS nanocrystals synthesized in the ratio of Zn/Y being 94/6%. The standard values of 2θ are 44.255˚and 51.867˚ corresponding to (012) and (015) planes respectively for a hexagonal structure as per PCPDS file no 72-0162. The most prominent peaks are obtained around 44.58˚ (012), smaller peaks are observed at 52.15˚ (015) lattice planes of hexagonal ZnS. The XRD patterns do not show any significant change due to doping with manganese or yttrium into ZnS nanocrystals. The peak obtained at 59.15˚ is due to zinc blende structure when doped with manganese [11]. However, this peak is not observed when doped with yttrium which is due to proper alloying of yttrium in the ZnS lattice. The mean crystallite sizes *D* were determined according to the Scherrer equation ($D = 0.9 \lambda / \beta \cos\theta$), where λ is the X – ray wavelength, β is the full width half maximum (FWHM) and θ is diffraction angle. λ for $CuK_\alpha$ radiation is 1.54060 Å The particle size distribution is found to be between 10 – 18 nm and the crystal structure is in hexagonal phase. The broadening of the XRD pattern takes place due to nanocrystalline nature of the sample.

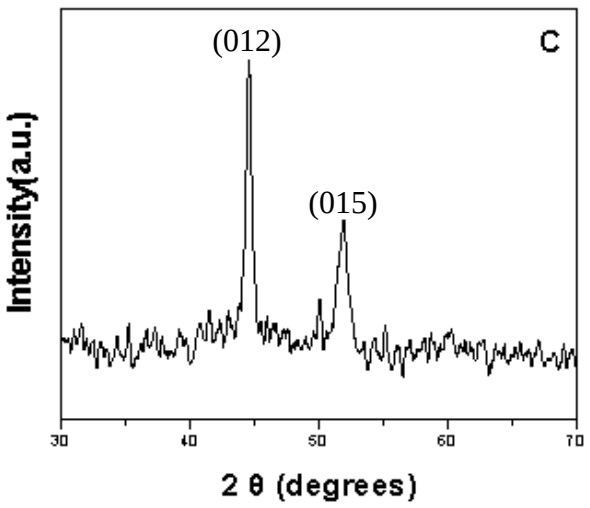


**Fig. 5.3(C)** *XRD pattern of drop coated film on Si substrate obtained from $Zn_{0.94}$ $Y_{0.06}S$ nanocrystals. The Bragg reflections are indexed.*

## 5.5 Fourier Transform Infra Red Spectroscopy

FTIR measurements have been made in the wave number range 1000 $cm^{-1}$ and 4000 $cm^{-1}$.

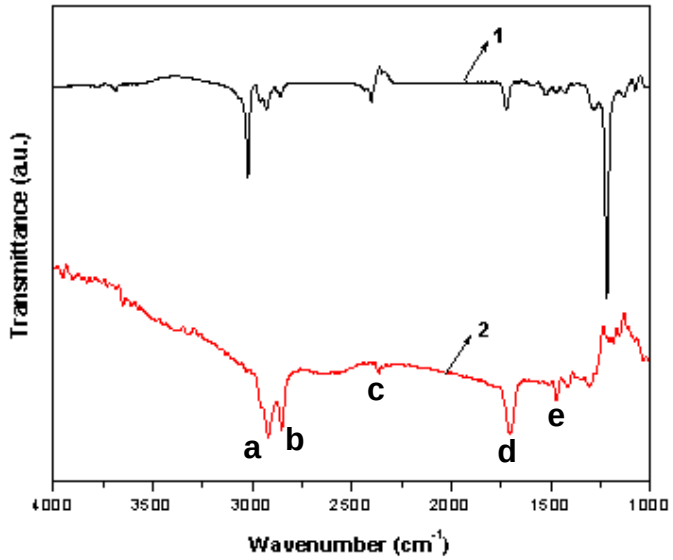


**Fig. 5.4(A)** *FTIR spectra recorded from drop coated film on Si(111) Wafer of ZnS nanoparticles (1) and 5% Mn doped ZnS nanocrystals (2).*

The FTIR characteristics of undoped ZnS (curve 1) and 5% manganese doped ZnS (curve 2) is shown in fig. 5.4(A).

Bands around 3000-3600 $cm^{-1}$ are due to hydrogen stretching frequency (OH stretching) (a). Bands around 1000-1500 $cm^{-1}$ are due to oxygen stretching and bending frequency (e). Bands near 1100 to 1050 $cm^{-1}$ are assigned to symmetric and asymmetric stretching. Bands near 1200 and 1100 $cm^{-1}$ are due to characteristic frequency of inorganic ions (d). Bands near 2600-2500 $cm^{-1}$ are assigned to S–H stretching vibration(b). The FTIR characteristics of ZnS nanoparticles (curve 1), 2% yttrium doped ZnS (curve 2) and 6% yttrium doped ZnS nanoparticles (curve 3) are shown in fig. 5.4(B).

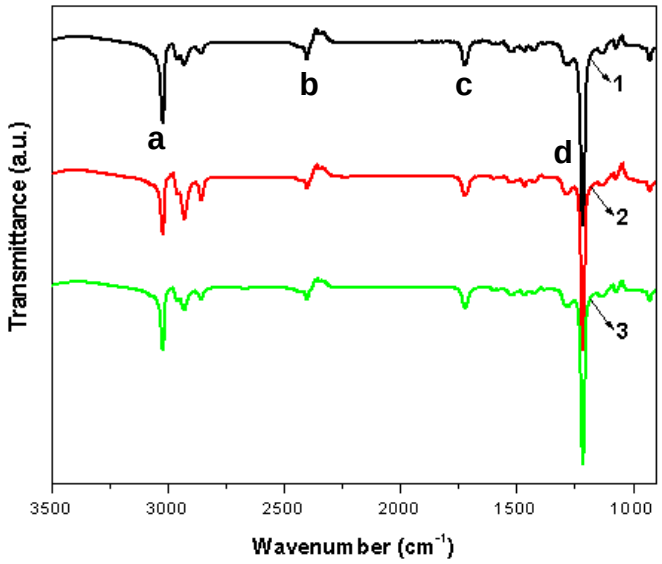


**Fig. 5.4(B)** *FTIR spectra recorded from drop coated film on Si(111) Wafer of ZnS nanoparticles (1), 2% Yttrium doped ZnS nanocrystals (2) and 6% Yttrium doped ZnS nanocrystals (3).*

Weak additional bands were observed at 850, 975 $cm^{-1.}$ These modes indicate the presence of resonance interaction between vibrational modes of sulphide ions in the crystal.

The absence of certain absorbtion bands in manganese doped ZnS nanoparticles indicates that the secondary structure is undisturbed. The shifting of the peak may be due to the strong interaction between the ZnS molecules and Mn molecules.

There are few absorption peaks at 1000-4000 $cm^{-1}$ indicating that the prepared nano-ZnS is a good infrared-transmittance material.

## 5.5 Transmission Electron Microscopy (TEM) Measurements

Fig. 5.5 shows the High Resolution TEM (HRTEM) micrographs recorded from the as-prepared ZnS nanoparticles in organic phase.

It is apparent that the ZnS nanoparticles are spherical in nature. The size of the nanoparticles seems to be in the range of 5-10 nm. The figure shows nearly distribution of spherical nanoparticles.

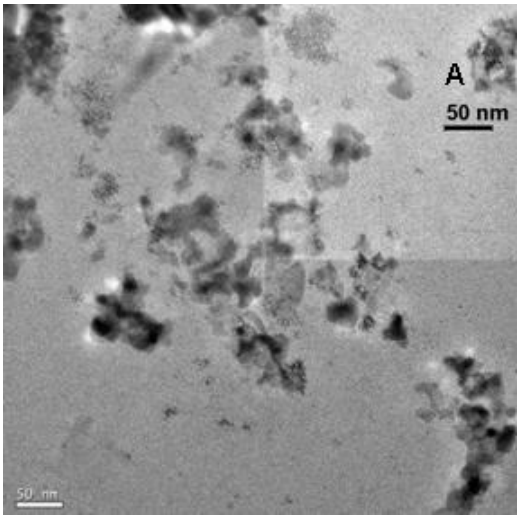


**Fig. 5.5** *HRTEM micrographs recorded at from as-prepared ODT capped ZnS nanoparticles.*

Fig. 5.6 illustrates the High Resolution TEM micrographs of 6% yttrium doped ZnS nanoparticles. It can be seen that the nanoparticles so synthesized are spherical in shape and show a size of 0.21nm and 0.33 nm. Doping has reduced the size and made the dispersion of the particles uniform. The highly dense structures clearly points out the strong surface binding of the ODT molecules with the ZnYS nanoparticles, thereby restricting their aggregation.

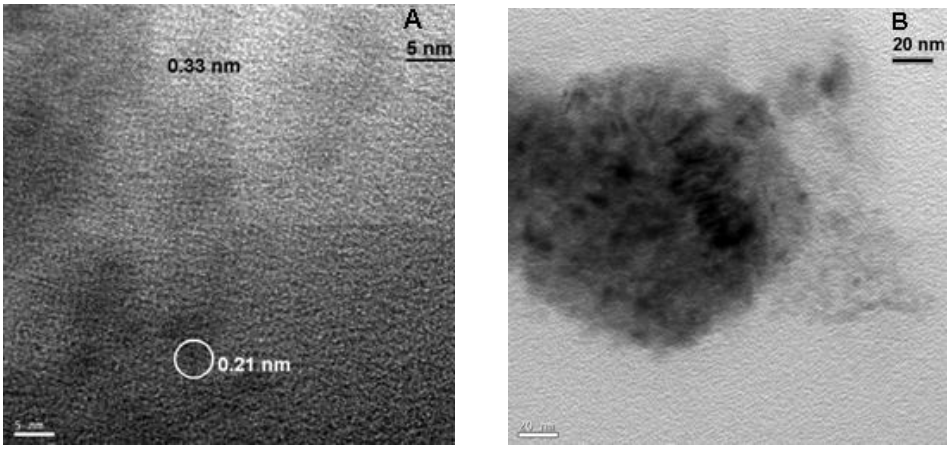


**Fig. 5.6** *HRTEM micrographs recorded at different magnifications from a drop cast film of ODT capped* $Zn_{0.94}$ $Y_{0.06}S$ *nanocrystals.*

## 5.6 Photoluminescence Measurements

The Photoluminescence spectrum of (PL) of ZnS nanoparticles are illustrated in figure 5.7(A), 5.7(B) and 5.7(C) for different excitation wavelengths.

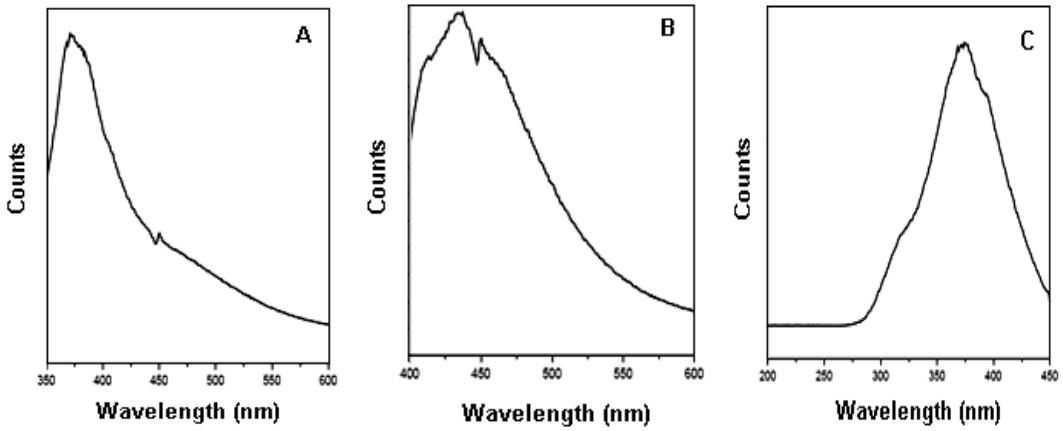


**Fig. 5.7** *PL spectra of ODT capped ZnS nanoparticles recorded with excitation wavelength of 320 nm* (**A**), *375 nm* **(B)** *and 465 nm* **(C).**

It is seen that the emission band from undoped ZnS nanoparticles is highly symmetric with increase in intensity due to homogeneous distribution of particles. The intensity of photoemission varies for different excitation wavelengths. The peak photoemission for an excitation wavelength of 320 nm is at 375 nm wavelength. The

peak photoemission for an excitation wavelength of 375 nm is at 430 nm wavelength. Similarly the peak photoemission for excitation wavelengths 465 nm is at 375nm wavelength. This is ascribed to a recombination of electrons at sulfur vacancy donor level with holes trapped at zinc vacancy acceptor level. The much weaker band at approximately 450nm is attributed to the defect related luminescence of the ZnS host lattice [18].

It is well known that semiconductor nanocrystals with the most perfect surface showed the most efficient photoluminescence [19], but the PL efficiency of semiconductor nanocrystals depends on the surface properties and is related to growing conditions and synthesis system [20]. The smaller particles have high surface to volume ratio and therefore contain more accessible carriers for photoluminescence.

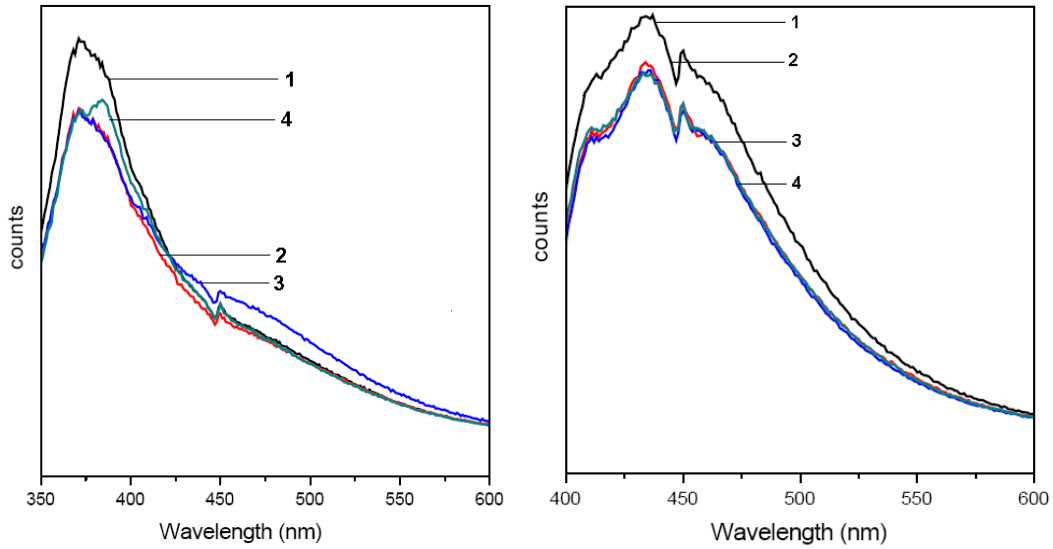


**Fig 5.8** *PL spectra of ODT capped ZnS nanoparticles (1), $Zn_{0.98}$ $Y_{0.02}S$ nanoparticles (2), $Zn_{0.94}$ $Y_{0.06}S$ nanoparticles (3) and $Zn_{0.9}$ $Y_{0.1}S$ nanoparticles (4) at an excitation wavelength of 330 nm (***A***) and 375 nm (***B***).*

In fig. 5.8, we have plotted the PL emission of undoped ZnS and yttrium doped ZnS for various concentrations of yttrium when the excitation wavelength of 330nm is used. The characteristics exhibit multiple peaks and the photoemission is

broadened. The peak photo emission occurs at around 375nm which is assigned to a recombination of electrons at sulfur vacancy donor levels with holes trapped at zinc vacancy acceptor level. No significant variation in the photoemission is found due to doping with yttrium. With the increase in $Y^{3+}$ doping concentration the quenching of blue emission band is observed and the emission in the yellow orange region takes place efficiently [17].

Multiple peaks are found in fig. 5.8(B) due to radiative recombination of the electrons and holes via surface states present in the nanocrystals [21, 22]. Fig. 5.9 illustrates the PL spectrum of undoped ZnS and yttrium doped ZnS at various concentrations of yttrium with an excitation wavelength of 465 nm. It shows peak emission at 370 nm and the intensity of photo emission is very high.

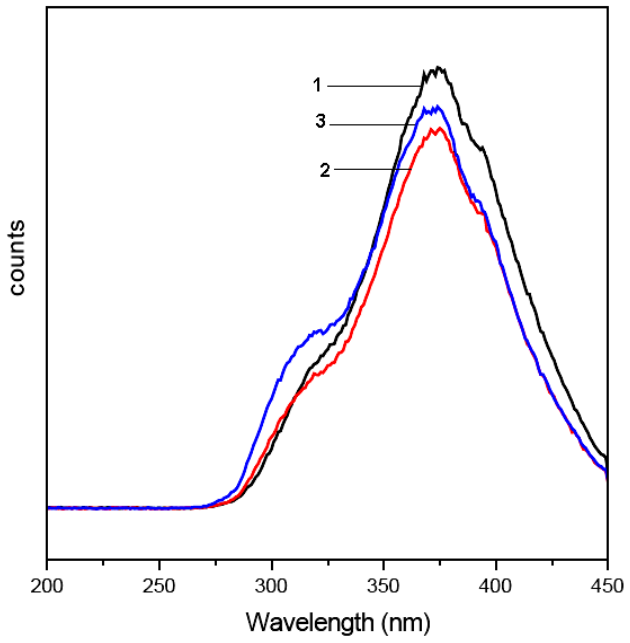


**Fig 5.9** *PL spectra of ODT capped ZnS nanoparticles (1), $Zn_{0.98}$ $Y_{0.02}S$ nanoparticles (2), $Zn_{0.94}$ $Y_{0.06}S$ nanoparticles (3) and $Zn_{0.9}$ $Y_{0.1}S$ nanoparticles (4) at an excitation wavelength of 465nm .*

It has also been observed that when ZnS nanoparticles are doped with different levels of manganese, the emission intensity is enhanced with the level of manganese

as the effective luminescent centers during the intensity from host lattice emission show a slow decrease.

## 5.7 Particle Size Distribution

The particle size measurements were performed to verify the size of the particles obtained using XRD and TEM. The particle shape is assumed to be spherical while measuring the size of the particles using the Malvern's particle size analyser and it has been confirmed using the TEM that particles are spherical in nature.

Figure 5.10 (A) presents the particle size distribution of undoped ZnS nanoparticles. All the particles have a size in the range of 100nm-200nm. This may be due to the agglomeration of the dispersed primary nanoparticles.

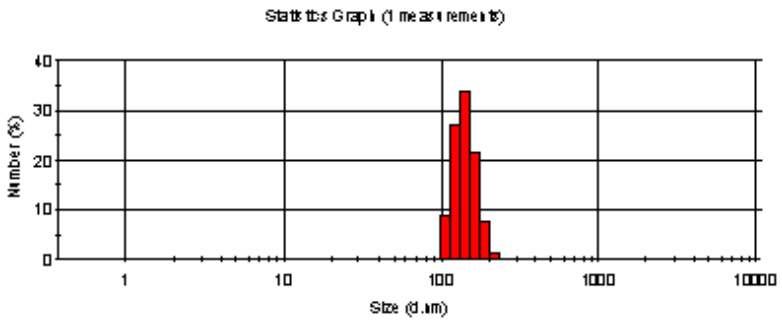


**Fig. 5.10(A)** *Histograms showing particle size distribution of ODT capped ZnS nanoparticles.*

The UV-vis absorption spectroscopy shows quantum confinement of the particles on doping. The fig. 5.10 (B) refers to 6% yttrium doped ZnS paticles. It can be concluded that the size of the nanoparticles synthesized reduces as the level of doping increases. To know the optimum level of doping where the particle size reduces, the concentration of yttrium was increased further and the particle size distribution obtained is illustrated in fig. 5.10 (B).

The increase in the doping level of yttrium causes a quantum confinement of the particles and size control can be achieved.

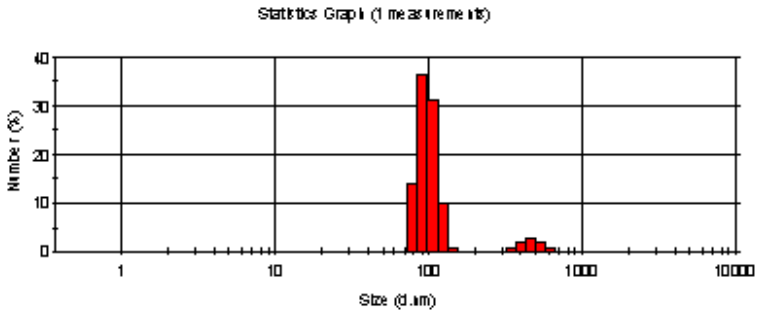


**Fig. 5.10 (B)** *Histograms showing particle size distribution of ODT capped* $Zn_{0.94}Y_{0.06}S$ *nanoparticles.*

Similarly particle size distribution of manganese doped zinc sulphide nanoparticles was characterized. Figures 5.10 (C) represent the particle size distribution of 5%, manganese doped ZnS nanoparticles.

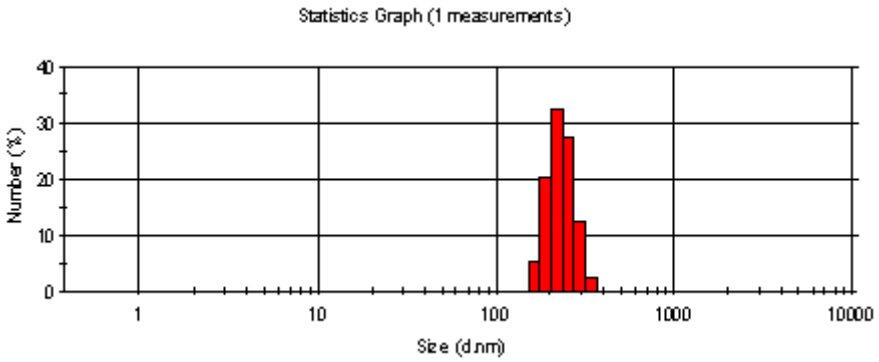


**Fig. 5.10 (C)** *Histograms showing particle size distribution of ODT capped* $Zn_{0.95}Mn_{0.05}S$ *nanoparticles.*

25% of the particles have a size less than 200 nm. This is due to certain level of aggregation that can be seen in the TEM also. All the particles are of the size less than 300 nm. The ZnS nanoparticles seem to aggregate more in comparison to CdS nanoparticles which exhibits a particle size of 100 nm. A significant reduction in the size can be observed when CdS is doped with manganese dopant.

Thus it can again be seen that the optimum level of doping with manganese is 5% where there is a significant change in the size of the nanoparticles synthesized compared to undoped ZnS nanoparticles illustrated in fig. 5.10 (A).

It can thus be concluded that the particle size distribution can be manipulated by doping and the extent of doping is very crucial. Doping beyond a certain level increases the size of the particles.

## 5.8 Summary

- Zn ions present in aqueous medium may be phase transferred into non-polar organic solvents by coordination with ODT molecules present in organic phase. The ODT molecules covalently bind to the ZnS nanoparticles surface. The most significant result in this experimentation is development of a system which allows the investigation of subtle surface state interaction and reactions of size quantized ZnS semiconductor particles in organic phase.
- UV- vis absorption and the band edge photoluminescence spectra are consistent with narrow size distribution and excellent particle quality. ZnS has good absorption for light in the wavelength of 220-350 nm and this peak position reflects the band gap of the particles. The fundamental absorption, which corresponds to electron excitation from the valence band to conduction band, can be used to determine the nature and value of the optical band gap of the prepared ZnS nanoparticles. This blue shifted absorption edge is due to small size of the particles.
- The study of particle size analysis reflects the effect of doping on the average size of the nanoparticles synthesized. Doping with manganese and

yttrium causes quantum confinement of the particles. The particle size distribution can be manipulated by doping and the extent of doping is very crucial. Doping beyond a certain level increases the size of the particles. The optimum doping percentage of manganese obtained was 6% in proportion with 94% of Zinc.

- The $Mn^{2+}$ ion, used as dopant in many luminescent materials exhibit a broad emission peak whose position depends strongly on the host lattice due to the crystal field strength with host. The emission colour can vary from green to deep red. Since a large portion of the atoms in nanocrystals is located on or near the surface, the surface properties should have significant effect on their structural and optical properties

- The smaller the size of quantum dots the higher the light emission efficiency they could provide. Therefore it is reasonable to expect that the synthesized products in this work could potentially be used in electroluminescent applications upon doping.

Thus, it can be seen that the chemical properties of manganese ions are very similar to those of zinc ions. Thus doping manganese into ZnS semiconductor is very favorable and enhances the band edge emission.

## 5.9 References:

[1] Davidson, W. L. *Phys. Rev.*, **1948**, *74, 116.*

[2] Rosetti, R.; Hull, R.; Gibson, J. M.; Brus, L. E. *J. Chem Phys.*, **1985,** *82, 552.*

[3] Brus, L. *J. Phys. Chem.*, **1986,** *90, 2555*.

[4] Henhlin, A. *Chem. Rev.*, **1989,** *89, 89.*

[5] Wang, Y.; Herron, N. *J. Phys. Chem.*, **1991,** *95, 525*.

[6] Khairutdinov, R. F. *Chemistry of semiconductor nanoparticles, Russian chemical reviews,* **1998,** *67 (2), 109.*

[7] Murugadoss, G.; Rajamannan, B.; Ramaswamy, V. *Journal of Lumin,* **2010,** *130, 2032.*

[8] Norris, D. J.; Bawendi, M. G. *Phys. Rev. B,* **1996,** *53, 16338.*

[9] Wang, L. W.; Zunger, A. *J. Phys. Chem. B,* **1998,** *102, 6449.*

[10] Ye Changhui; Fang Xiaosheng; Li Guanghai; Zhang Lide *Appl. Phys. Lett.,* **2004,** *85, 3035.*

[11] Chen, W.; Wang, Z.; Lin, Z.; Lin, L. *Appl. Phys. Lett.,* **1997,** *70, 1466.*

[12] Bhargava, R. N.; Gallagher, D.; Hong, X.; Numikko, A. *Phys. Rev. Lett.,* **1994,** *72, 416.*

[13] Bhargava, R. N. *J. Lumin,* **1996,** *70, 85.*

[14] Sarkar, R.; Tiwary, C.S.; Kumbhakar, P.; Basu, S.; Mitra, A.K. *Physica E,* **2008**, *40, 3115*.

[15] Chen Jianfeng; Li Yaling; Wang Yuhong; Yhun Jimmy; Cas Dapeng *Mater Res. Bull,* **2004,** *39, 185*.

[16] Brieler, F. J.; Froba, M.; Chen, L.; Klar, P. J.; Heimbrodt, W.; Krug Von Nidda, H. A.; Loidl, A. *Chem. Eur. J. ,* **2002,** *81, 185*.

[17] Sapara, S.; Prakash, A.; Ghangrekar, A.; Percasainy, N.; Sharma, D. D. *J. Phys. Chem B,* **2005,** *109, 1663*.

[18] Suyver, J. F.; Wuister, S. F.; Kelly, J. J.; Meijerrink, A. *Nano Lett.,* **2001**, *1, 426*.

[19] Talapin, D. V.; Rogach, A. I.; Shevchenko, E. V.; Kornowski, A.; Hasse, M.; Weller, H. *J. Chem.Soc.,* **2002,** *124, 5782*.

[20] Guo, J.; Yang, W.; Wang, C. *J. Phys. Chem. B,* **2005,** *109, 17467*.

[21] Liu, S. M.; Liu, F. Q.; Guo, H. Q.; Zhang, Z. H.; Wang, Z. G. *Solid state Commun*, **2000,** *115, 615*.

[22] Nag, A.; Sarma, D. D. *J. Phys Chem C let.*, **2007,** *111, 13641*.